17

Survey of Recent Volumetric Medical Image Segmentation Techniques

Hu[1], Grossberg[2] and Mageras[1]
[1]*Memorial Sloan-Kettering Cancer Center, New York*
[2]*City College of New York, New York*
USA

1. Introduction

The goal of medical image segmentation is to partition a volumetric medical image into separate regions, usually anatomic structures (tissue types) that are meaningful for a specific task. In many medical applications, such as diagnosis, surgery planning, and radiation treatment planning, determination of the volume and position of an anatomic structure is required and plays a critical role in the treatment outcome.

1.1 Problem domain

Volumetric medical images are obtained from medical imaging acquisition technology, such as CT, MRI, and PET, and are represented by a stack of 2D image slices in 3D space. The tissue type surrounding the voxel determines its value. Within a volumetric medical image, the variations in tissue type give rise to varying intensity. Typically this intensity is a quantized scalar value also known as a gray level. While it is possible to consider more general cases such as vector or tensor values, we will confine our discussion to the scalar case. The segmentation problem is essentially a classification problem. A label representing the region to which an image voxel belongs is assigned to each voxel. The assignment is, however, subject to some constraints, such as piecewise continuity and smoothness; thus, classification is difficult due to image acquisition artifacts.

1.2 Survey outline

This survey includes several fundamental image segmentation techniques that are widely used in the area of computer vision with application to medical images. It also includes recent developments over the last ten years that are based on these techniques. In particular, this survey focuses on the general techniques that are not specific to certain anatomic organ structure, techniques that are easily expandable to 3D, and techniques that can flexibly make use of statistical information.

In this survey, segmentation techniques are broadly categorized into four groups (Fig. **1**), according to the use of image features: region-based, boundary-based, hybrid, and atlas-based. Typically, region-based and boundary-based techniques exploit within-region

Fig. 1. The four categories of medical image segmentation techniques and their selected methods discussed in this survey.

similarities and between-region differences, respectively, whereas hybrid techniques use both region and boundary-image features, and atlas-based techniques involve image registration between an atlas and the image to be segmented. These four groups of techniques are discussed in detail in sections 2, 3, 4, and 5. Many of these methods use optimization techniques and partial differential equations (PDE). The optimization methods and the solutions to PDEs, however, are beyond the scope of this survey. Finally, the advantages and disadvantages of various types of techniques are discussed in section 6.

1.3 Notations

The following notations are used throughout the entire survey. An image f is defined over its discrete image domain Ω as

$$f(x) \in \Re, x \in \Omega \subset \Re^3 . \quad (1)$$

Let r_i, $i = 1,\ldots,K$, be the labels representing K regions in the image. A segmentation g is defined over the image domain as

$$g(x) \in \{r_i \mid i = 1,\ldots,K\} . \quad (2)$$

Finally, $R_i = \{ x \mid g(x) = r_i \}$, $i = 1, \ldots, K$ are the K regions.

2. Region-based methods

In region-based methods, a region can be defined by a predicate function P based on some homogeneous property such that all voxels in a region satisfy the homogeneity criteria, that is:

$$P(R_i) = \text{true}, i = 1,...,K \ . \tag{3}$$

Segmentation is the partition of an image Ω into K disjoint regions such that the following conditions are satisfied:

$$\Omega = \bigcup_{i=1}^{K} R_i , \tag{4}$$

$$R_i \cap R_j = \{\}, i \neq j, \tag{5}$$

$$P(R_i \cup R_j) = \text{false}, \ i \neq j. \tag{6}$$

Eq. (6) states that the predicted outcome is different for any two different regions. Region-based methods can be further categorized into five groups based on how the rules of prediction are carried out: thresholding, region growing, region splitting and merging, and classification.

2.1 Thresholding

Thresholding is the simplest and fastest region-based method. A region label is assigned to a voxel by comparing its gray-level value to one or multiple thresholds. Thresholding can be global, when a constant threshold is applied to whole image, or local or dynamic, when a different threshold is used for different regions in the image. For simplicity and without loss of generality, we assume a global single threshold θ is used to segment the image into two regions: 0:*foreground* and 1:*background* (when applicable, this two-class assumption will be applied to other methods discussed in this survey).
A predicate function P can be defined as follows:

$$\begin{aligned} P(R_0) &= \textbf{true, if } \forall x \in R_0, f(x) \geq \theta, \\ P(R_1) &= \textbf{true, if } \forall x \in R_1, f(x) < \theta. \end{aligned} \tag{7}$$

Thus, the following rules are used for segmentation:

$$g(x) = \begin{cases} r_0 & \text{if } f(x) \geq \theta, \\ r_1 & \text{otherwise.} \end{cases} \tag{8}$$

2.2 Choosing thresholds

The key factor that affects the segmentation result is the choice of threshold value. Thresholds are usually determined by consulting a histogram. For a medical image, a threshold can be obtained from a priori knowledge. In the case of CT images, voxel intensities are given in Hounsfield Units (HU), and the ranges of HU for certain tissue types are known (Table 1). For example, air is -1000, water is 0, and bone is usually larger than 250.

	Hounsfield Unit	
Tissue	Low	high
Air	-1000	-1000
Water	0	0
Fat	-150	-10
Muscle	10	50
Bone	250	1000
Lung	-100	-1000
Liver	40	60
Kidney	30	50

Table 1. Hounsfield unit range for various tissue types

Thresholds can also be chosen automatically. The automatic approaches can be further separated into two groups. One group selects the threshold based on analyzing the shape of the histogram. The other group finds the optimal thresholds by minimizing or maximizing some merit function.

2.2.1 Based on analyzing peaks and valleys of the histogram

Assuming that the distribution is a bi-modal histogram, one can find the threshold by finding its peaks and valleys. Rosenfeld and Torre (1983) analyze concavities by constructing a convex hull of the histogram and calculating the difference between the histogram and its convex hull. The threshold is chosen by locating the maximum difference (Fig. **2**). It can be described as follows:

$$\theta_{concavity} = \arg\max_{\theta}\{\,|h(\theta) - h^{hull}(\theta)|\,\}\,, \tag{9}$$

where h is the intensity histogram of the image.

Sezan (1990) carried out peak analysis by convolving the histogram with a smoothing kernel for reducing sensitivity to noise and a differencing kernel for locating the peaks. The kernel operation produces the peak detection signal. The start of a peak is indicated as the gray level at which the detection signal has a zero-crossing to negative values represented by s_i, and the end of peak e_i is defined to be the gray level at which the detection signal attains its the local maximum between the starts of the two adjacent peaks. The thresholds can be set anywhere between the two adjacent peaks, that is:

$$T_{sezan} = \{\theta_t \,|\, \theta_t = \lambda e_i + (1-\lambda)s_{i+1}, i = i,...,K, 0 \le \lambda \le 1\}\,. \tag{10}$$

Variations on this theme that apply to MR brain image segmentation are provided by Aboutanos et al. (1999), who obtain a smoothed histogram via a Gaussian kernel followed by curvature analysis of the presence of both valleys and sharp curvature points corresponding to gray and white matters.

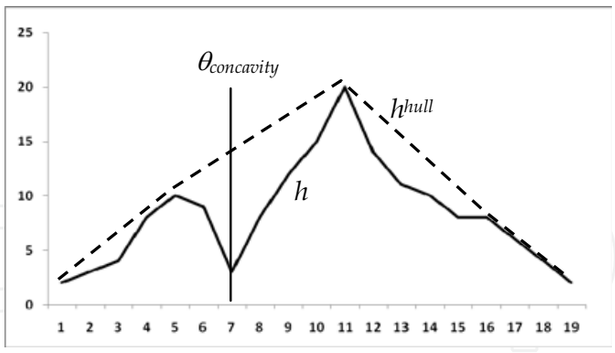

Fig. 2. A histogram h and its convex hull h^{hull}. The optimal threshold $\theta_{concavity}$ is chosen as the point at which the distance between the histogram and its convex hull is maximal.

2.2.2 Optimal thresholding

When the threshold is chosen automatically, it is usually done so by applying some measure of merit or objective function on the resulting partition. A special case of this is to apply the measure of merit on the division of the image histogram resulting from the threshold. Otsu (1979) minimizes within-class variance, which is equivalent to maximizing between-class variance:

$$\begin{aligned}&\sigma_B^2(\theta) = \sigma^2 - \sigma_W^2(\theta)\\ &= \sum_{k<\theta} p(k)(\mu_0 - \mu)^2 + \sum_{k\geq\theta} p(k)(\mu_1 - \mu)^2 ,\\ &\theta_{Otsu} = \arg\max_{\theta}\{\sigma_B^2(\theta)\}\end{aligned} \tag{11}$$

where probability density $p(k)$ is obtained from the histogram, and μ_1, μ_2, and μ are the mean of the two classes ($k < \theta$ and $k \geq \theta$) and the global mean, respectively. In some forms of medical images, like CT and MR, the gray levels are discrete and finite, and therefore the optimal threshold can be found by evaluating all the bins of the histogram. Kapur et al. (1985) maximized the sum of the two classes of Shannon entropies:

$$\theta_{Kapur} = \arg\max_{\theta}\{-\sum_{i\leq\theta}\frac{p(i)}{\sum_{i<\theta}p(i)}\log(\frac{p(i)}{\sum_{i<\theta}p(i)}) - \sum_{i>\theta}\frac{p(i)}{\sum_{i\geq\theta}p(i)}\log(\frac{p(i)}{\sum_{i\geq\theta}p(i)})\} , \tag{12}$$

Ridler and Calvard (1978) introduced an iterative method that finds the optimal threshold such that the threshold is equidistant to the two class means. The iterative algorithm is described below:

Algorithm: Ridler & Calvard iterative method

1. Given an initial θ^0. For example, $f_{\max}/2$.
2. At iteration i, compute the 2 class means and threshold

$$\mu_0^{(i)} = mean\{f(x) \mid f(x) < \theta^{(i)}\},\ \mu_1^{(i)} = mean\{f(x) \mid f(x) \geq \theta^{(i)}\}$$
$$\theta^{(i+1)} = \left(\mu_0^{(i)} + \mu_1^{(i)}\right)/2$$

3. repeat 2 until $|\theta^{(i+1)} - \theta^{(i)}|$ become suffciently small.

This algorithm is quite similar to the procedure used in K-means clustering, but as applied to the image histogram. Clustering methods are discussed in section 2.5.

2.3 Summary of thresholding methods

The simplicity of thresholding methods leads to implementations that are extremely fast and can even be implemented in hardware. The thresholds can be chosen using prior knowledge or analyzing the shape of the histogram, or by finding optimal ones based on clustering. If the threshold is chosen using only the image histogram then the method will not be senstive to volume preserving transformations. However, it is sensitive to image artifacts that alter the true intensity distribution. For more complete information about threshold selection, readers are referred to Sezgin and Sankur (2004).

2.4 Region growing

Region growing starts with seeds on the images. Each seed represents a region. The region grows by successively adding neighboring voxels based on the homogeneity predicate. A generic region growing algorithm for one region is given below:

Algorithm: Region Growing
RegionGrow(*seed*)
1. region $r = \{seed\}$
2. while $r.neighbors \neq \{\}$
   for each voxel x in $r.neighbors$, if $P(x,r) =$ true then $r.add(x)$.
   end while
3. return r

In seeded region growing, seed selection is decisive and is often done manually in medical image applications. The difference between the many seeded region-growing methods lies in the definition of the homogeneity criteria. Adam and Bischof (1994) use the distance between the voxel value and the region's mean value. Thus, they define a predicate as

$$P(x,r) = \left| f(x) - \mu_r \right| < T, \tag{13}$$

where T is a threshold that can also be chosen manually or even interactively, since the mean can be calculated very quickly. Instead of growing a single region, Adam's seeded region growing also examines the situation of growing multiple disjoint regions. A set of boundary voxels can be defined as

$$B = \{x \mid x \notin \bigcup_i R_i, N(x) \cap \bigcup_i R_i \neq \phi\}, \tag{14}$$

where $N(x)$ is neighbors of voxel x. During the growing steps, a voxel is chosen from B and added to the region r if the distance measure $|f(x) - \mu_r|$ as defined in Eq. (13) is the smallest among all regions.

Unseeded region growing was proposed by Lin et al. (2001), and their method does not need region seed point initialization. The method starts with an arbitrary voxel and assigns it to a region and grows the region using the generic region growing algorithm. If a neighboring voxel does not meet the homogeneity criteria for the region, then the method uses Adam's method to add the voxel to another region that has the minimum distance to

the voxel while maintaining the homogeneity criteria for that region. If such a region does not exist, then a new region is created for the voxel and the new region starts growing as well. The solution found might not be the optimal one, because a voxel might not be added to the most closely related region if that region is created after the voxel was visited. It may be necessary to re-evaluate the neighborhood of any newly created region.

2.5 Region splitting and merging

A different approach to region growing is region splitting and merging. The method was presented by Horowitz and Pavlidis (1974). An image is initially split into four sub-images (eight in 3D) if it does not meet some homogeneity criteria, e.g., in their method, $|\max f_R(x) - \min f_R(x)| < T$. The sub-image relationships can be represented as a quadtree (or octree in 3D). When a new region (sub-image) is created, it is checked to determine whether it can be merged with its siblings if they have the same homogeneity properties. This is done recursively on each sub-image until splitting and merging is no longer possible. The final step merges adjacent regions across parent nodes that meet the uniformity criteria. The resulting algorithm is presented below:

Algorithm: Region Splitting and Merging
RegionSplitMerge(R)

1. Split R into four (or eight in 3D) sub-regions if it does not meet the homogeneity criteria. Merge children sub regions of the same parent node that meet these criteria. If no splitting and merging possible, then return.
2. For each sub region R_i, RegionSplitMerge(R_i).
3. If $R=\Omega$ (finished for the whole image), check adjacent regions in the quadtree (octree) across parent nodes and merge those that meet the homogeneity criteria.

2.6 Summary of region growing and splitting and merging

These methods are less sensitive to image noise then thresholding methods because of the use of regional properties and the resulting segmentation is piece-wise continuous. Some region homogeneity criteria involve thresholds as well. However, if the region mean is used as the homogeneity measure, since it can be calculated efficiently, the threshold can be

Fig. 3. CT liver segmentation using region growing shows boundary leakage. The seed point is marked as a cross.

selected interactively to obtain suitable segmentation. These methods perform quite well when segmenting organs, such as lungs or bony structures, that have well-defined boundaries. Boundary leakage remains problematic for these methods with structures having blurred boundaries (**Fig**. **3**.) Type of splitting used and initial seed points are factors to the results. The results need not be translation or rotation independent. With these methods it is hard to state clearly what objective function or measure of merit the final result minimizes.

2.7 Classification methods

This section describes a number of common techniques used for pattern recognition. It does not cover all classification techniques, but rather focuses on techniques widely used in medical image segmentation. This includes unsupervised clustering algorithms, such as *K-means* and *fuzzy c-means*, and supervised Bayesian methods, such as maximum likelihood and Markov random fields.

2.7.1 Clustering

Similar to image segmentation, clustering involves dividing a set of objects into groups (clusters) so that objects from the same group are more similar to each other than objects from different groups. Often, similarity is determined by a distance measure, such as the Euclidean distance or Mahalanobis distance. Given a known number of clusters K and number of data points N, the matrix

$$U_{K\times N} = \left[u_{ki}\right], k = 1,...,K \text{ and } i = 1,...,N \,, \tag{15}$$

represents the partitions of the data set, where u_{ki} describes the membership of data point x_i in cluster c_k. The clustering is considered *hard* if u_{ki} is either 1 (is a member of) or 0 (is not a member of) and is determined by Boolean membership functions; or as *fuzzy* if partial membership is allowed with continuous membership functions. Let v_k be the centroid of cluster c_k. Then v_k can be calculated from

$$v_k = \sum_{i=1}^{N} u_{ki} x_i \,/\, \sum_{i=1}^{N} u_{ki} \,, k = 1,...,K \,. \tag{16}$$

2.7.1.1 K-means

K-means is also called hard c-means. The membership value u_{ki} must satisfy

$$\forall k, \forall i, u_{ki} = \{0,1\}, \forall i, \sum_{k=1}^{K} u_{ki} = 1, \text{and } \forall k, 0 < \sum_{i=1}^{N} u_{ki} < N. \tag{17}$$

By defining a distance function d_{ki}, for example, the Euclidean distance is

$$d_{ki} = \left\| x_i - v_k \right\| , \tag{18}$$

then the task is to find U that satisfies the membership constraints in (16) and minimizes

$$J(U,v) = \sum_{k=1}^{K} \sum_{x_i \in c_k} {d_{ki}}^2 \,. \tag{19}$$

A common way to find U is by using the iterative method was proposed by Lloyd (1982). The algorithm is described below:

Algorithm: *K*-means clustering
1. Given number of clusters K, initialize centroid v_k for each cluster k randomly or heuristically.
2. Calculate each u_{ki} in membership matrix U. $u_{ki} = 1$ if x_i is closest to cluster k based on the selected distance measure d (e.g. Eq. 18), otherwise $u_{ki} = 0$.
3. Recalculate cluster centroids from U using Eq. 16.
4. Repeat 2-3 until all cluster centroids (or matrix U) are unchanged since the last iteration.

2.7.1.2 Fuzzy c-means

Fuzzy c-means (FCM) is a generalization of k-means. Unlike hard membership in k-means, it allows the data points to be partially associated with more than one cluster , showing a certain degree of membership to each cluster. The membership value u_{ki} must satisfy:

$$\forall k, \forall i, 0 \le u_{ki} \le 1, \forall i, \sum_{k=1}^{K} u_{ki} = 1, \text{and } \forall k, 0 < \sum_{i=1}^{N} u_{ki} < N. \tag{20}$$

Note that these conditions only differ from k-means' in the first condition.

One of the most widely used FCM algorithms was proposed by Bezdek (1981). In this algorithm, the objective function to be minimized is

$$J_m(U, v) = \sum_{k=1}^{K} \sum_{x_i \in c_i} {u_{ki}}^m {d_{ki}}^2 . \tag{20}$$

where $m \ge 1$ controls the degree of fuzziness. The larger the m, the fuzzier the membership assignments. If m is close to 1, then the cluster with centroid closest to the point is given more weight than the other clusters. Unlike hard membership in k-means, the membership value and centroid are calculated as follows:

$$u_{ki} = \sum_{j=1}^{K} \left(\frac{d_{ki}}{d_{ji}} \right)^{-2/(m-1)} , \tag{21}$$

$$v_k = \sum_{i=1}^{N} {u_{ki}}^m x_i \Big/ \sum_{i=1}^{N} {u_{ki}}^m . \tag{22}$$

The iterative algorithm is similar to the k-means algorithm in 2.7.1.1, except that Eqs. (21) and (22) are used for calculating U and the centroids, and the algorithm stops when

$$\max\left(\left| {u_{ki}}^{(n)} - {u_{ki}}^{(n-1)} \right| \right) < \varepsilon, \text{ for some constant } \varepsilon . \tag{23}$$

For medical image segmentation, some spatial constraints may be needed in order to generate regions that have piecewise continuity. Fig. 4 shows the comparison of segmentations of noisy brain images using fuzzy c-means with and without spatial information.

Several approaches address this problem. Pham (2002) added a penalty term in Eq. 20 for inconsistency assignments in the local neighborhood of a voxel. If voxel i is assigned to cluster k, the penalty term is the sum of the voxel i's neighbors' membership values of clusters other than cluster k, as defined below

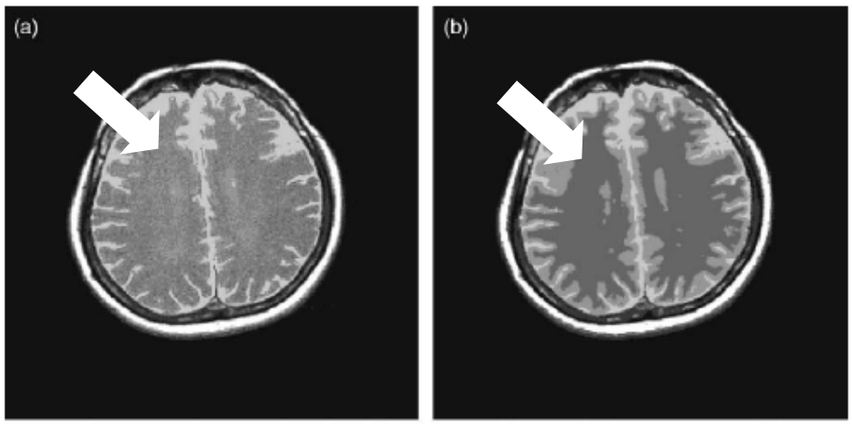

Fig. 4. (a) fuzzy c-mean segmentation without a spatial constraint (b) with a spatial constraint to preserve the piecewise continuity (arrows). Reprint from Chuang et al. (2006) with permission from Elsevier.

$$\frac{\beta}{2}\sum_{i=1}^{N}\sum_{k=1}^{K}u_{ki}{}^{m}\sum_{j\in N_i}\sum_{q\in Q_k}u_{qj}{}^{m}, \text{where } Q_k=\{1,...,K\}\setminus\{k\}\ . \tag{24}$$

Mohamed et al. (1999) modified the distance measure by incorporating the cluster assignments of neighboring voxels weighted by the distance between the reference voxel and its neighbor. The distance measure is defined below:

$$d_{ki}=d_{ki}(1-\alpha\sum_{j\in N_i}u_{kj}p_{ij}/\sum_{j\in N_i}p_{ij}), \text{where } p_{ij}=\left|x_i-x_j\right|. \tag{25}$$

With this distance measure, the total effect of the neighboring pixels pulls their neighbor toward the same class.

2.7.1.3 Summary of clustering methods

Clustering methods are suitable for segmenting a site where the means of the intensity distributions of the tissue types are well separated. A common application is MRI brain image segmentation. The centers of T1-T2 intensity clusters of white matte (W), gray matter (G), cerebrospinal fluid (C), air (A) and fat (F) are shown in Fig. **5**. In addition, a spatial constraint is needed to overcome the noise artifact. Since the data is grouped by positions in a feature space, there is no guarantee that points on the same cluster need to be close spatially. It is possible to add position into the feature space but this introduces the requirement of specifying a prior to balance continuity in feature space (homogeneity) with continuity in space (proximity.)

2.7.2 Bayesian

Bayesian approaches treat the class assignment of the voxels as random variables and rely on probability to derive probabilistic models for images. Usually, Bayesian decision theory is the tool for classification. Here we slightly change the notation. Let x_i be the random

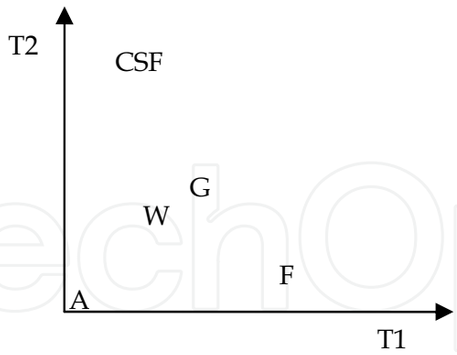

Fig. 5. Centers of clusters of T1-T2 intensity of various tissue types in an MRI brain image.

variable for class assignment of voxel i, let y_i be the random variable for an image feature (e.g., intensities) at voxel i, and let w_k represent the class k, k = 1,…,K.

2.7.2.1 Maximum Likelihood (ML) and Expectation Maximization (EM)

Maximum likelihood methods assume that the voxel intensities are independent samples from a mixture of probability distributions of classes. For a Gaussian mixture model, the set of class parameters are

$$\theta = \{\theta_k \mid \theta_k = (\mu_k, \sigma_k, P(\omega_k)), k = 1,...,K\}, \tag{26}$$

where μ_k is the mean, σ_k is the standard deviation and $P(\omega_k)$ is the prior for class k.
The maximum likelihood estimation problem is, given some observed data y, find the θ that makes the data most likely, that is

$$\theta^* = \arg\max_{\theta} P(Y = y \mid \theta). \tag{27}$$

The likelihood function is given by

$$L(\theta) = p(y \mid \theta) = \prod_{i}^{N} p(y_i \mid \theta) = \prod_{i=1}^{N} \sum_{k=1}^{K} p(y_i \mid w_k, \theta_k) p(w_k) \tag{28}$$

Since y is the observed data and is fixed, the likelihood function is viewed as a function of θ. When estimating the mixture model parameters, a good method is the EM algorithm discussed by Dempster et al. (1977). The algorithm is an iterative procedure:

Algorithm: EM algorithm for maximum likelihood estimation of Gaussian mixture model

1. Initial θ, $p(y_i \mid w_k, \theta_k)$ and $p(w_k), k = 1,..,K$, are given from training data or obtained from a histogram.
2. *E-Step*
   Calculate $p(w_k \mid y_i, \theta)$ based on Bayes' rule:

$$p(w_k \mid y_i, \theta) = \frac{p(y_i \mid w_k, \theta) p(w_k)}{\sum_{j=1}^{K} p(y_i \mid w_j, \theta_j) p(w_j)}$$

3. *M-Step*

Let $f_{ki} = p(w_k \mid y_i, \theta)$ obtained in *E-step* . Calculate new $P(w_k), \mu_k, \sigma_k$ as follows:

$$p(w_k) = \frac{1}{N}\sum_{i=1}^{N} f_{ki}, \mu_k = \frac{\sum_{i=1}^{N} y_i f_{ki}}{\sum_{i=1}^{N} f_{ki}}, \text{and } \sigma_k = \frac{\sum_{i=1}^{N} (y_i - \mu_k)^2 f_{ki}}{\sum_{i=1}^{N} f_{ki}}$$

4. Repeat *E-Step* and *M-Step* until θ does not change.

2.7.2.2 Maximum a posteriori (MAP) and Markov Random Field (MRF)

Using Bayes's rule, the a posteriori probability is given as

$$p(x \mid y) = \frac{p(y \mid x)p(x)}{p(y)}. \tag{29}$$

Since y is observed and fixed, we get

$$p(x \mid y) \propto p(y \mid x)p(x). \tag{29}$$

Maximizing the a posteriori (MAP) estimation is equivalent to maximizing $p(y \mid x)p(x)$. Again, if independence between voxels is assumed, the optimal segmentation is obtained by

$$x^* = \arg\max_x \sum_{i=1}^{N} \log(p(y_i \mid x_i)) + \log(p(x)). \tag{30}$$

The prior $p(x)$ can be modeled by an undirected graphical model-Markov Random Field (MRF) (Basag 1986; Geman and Geman 1984; Grieg et al. 1989). By the Hammersley-Clifford theorem, the prior can be written as a product of *clique potential functions* as follows:

$$p(x) = \frac{1}{Z}\prod_c \psi_c(x_c). \tag{31}$$

where c are the maximum cliques in the graph, and ψ_c is strictly positive. Thus, it is usually expressed as an exponential:

$$\psi_c(x_c) = \exp(-E(x_c)). \tag{32}$$

where E is called an energy function.

Considering the image domain based on the lattice structure with a four-connected (2D) (Fig. 6) or six-connected (3D) neighborhood system, by definition, the maximum clique consists of two neighboring voxels. Thus, we can define an energy function for the clique at each voxel i in terms of functions φ_1 and φ_2:

$$E(x_i) = \alpha\varphi_1(x_i) + \beta \sum_{j \in N_i} \varphi_2(x_i, x_j). \tag{33}$$

For simplicity, we set α to 0. Finally, we can rewrite Eq. (30) as

$$x^* = \arg\max_x \sum_{i=1}^{N} \log(p(y_i \mid x_i)) - \beta \sum_{i=1}^{N} \sum_{j \in N_i} \varphi_2(x_i, x_j). \tag{34}$$

To achieve the piecewise continuity preferred in the segmentation, φ_2 can be simply defined as a delta function to penalize the discontinuity:

Fig. 6. Sub-graph at node i in the 2D lattice image. Each pair of {*i*, *j*}, $j \in N_i$, is a maximum clique.

$$\varphi_2(x_i, x_j) = \delta(x_i, x_j) = \begin{cases} 1 & \text{, if } x_i \neq x_j \\ 0 & \text{, otherwise.} \end{cases} \tag{35}$$

The maximization is usually done by *simulated annealing* or the *iterated conditional modes* (ICM) algorithm (Basag 1986). However, if the segmentation is a two-class problem, it can be done using a graph *min s-t cut* algorithm (Greig et al. 1989). A graph with N+2 nodes is constructed from an image grid. The additional two nodes *s* and *t* represent the two classes. Each node is connected to *s* and *t* and its neighbors with edges. The cost of each edge is assigned based on the first term and second term defined in Eq. (34). Fig. **7** shows the edge cost assignment. The maximization can then be obtained by finding the min s-t cut; and the nodes are partitioned into two groups, with one group remaining connected *s* representing a class and the other group remaining connected to *t* representing the other class. Kolmogorov and Zabih (2004) studied the energy functions that can be minimized using a graph cut.

3. Boundary-based methods

In this section, the survey focuses on deformable models that are widely used and studied in medical image segmentation because of their contour connectivity.

Deformable models are curves or surfaces defined in an image domain that change their shape under the influence of force. The forces are usually *internal*, from the curve or surface itself, or *external*, from the image data. Boundary-based methods can be divided into two groups, depending on how the curve and surface are defined: the parametric (explicit) deformable model, which is also called active contour; and the non-parametric (implicit) deformable model, which is also called level set or geometric active contour.

3.1 Parametric deformable model (active contour)

Active contours, also known as "snakes" (Kass et al. 1988), are parametric curves represented by $c(s) = (x(s), y(s))$, $0 \le s \le 1$, in the 2D image domain (for simplicity). The model is active because it always minimizes the following energy function as the shape of the contour changes

$$E(c) = \int_0^1 E_{in}(c(s)) + \lambda E_{ex}(c(s))ds \, . \tag{36}$$

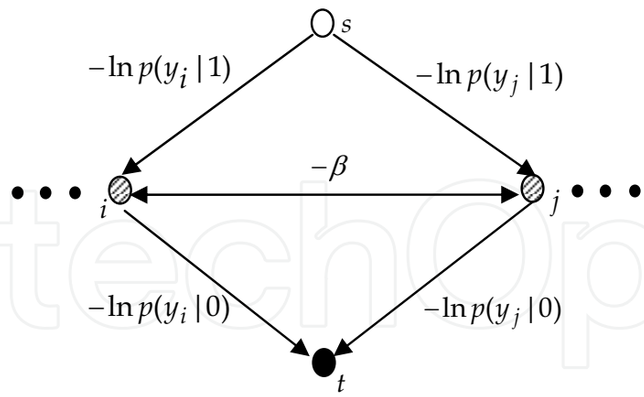

Fig. 7. Edge cost assignment for the graph cut based segmentation. Finding the minimum cost of its *s*-*t* cut is equivalent to maximizing the objective function in Eq. (34).

Here, E_{in} is the internal energy due to the bending of the contour, and E_{ex} is the external energy from the image data and external constraints. λ is a weighted constant. E_{in} can be written:

$$E_{in} = \left(\alpha(s)\left|c'(s)\right|^2 + \beta(s)\left|c''(s)\right|^2 \right) / 2 \,. \tag{37}$$

The internal energy is meant to enforce the smoothness of the curve and is composed of a first-order term c' controlled by $\alpha(s)$ and a second-order term c'' controlled by $\beta(s)$. The second-order term causes the snake to act like a thin-plate. Setting a point to zero allows the snake to build up a corner around the point. In practice, $\alpha(s)$ and $\beta(s)$ are often chosen to be constants. The external energy can be the image force that attracts the contour toward some image features, like edges, as defined below:

$$E_{ex} = -\left|\nabla f\right| . \tag{38}$$

To reduce the noise artifacts and extend the range of the image force, we can use edges on an image smoothed with a Gaussian kernel:

$$E_{ex} = -\left|\nabla\left(G_\sigma * f\right)\right| . \tag{39}$$

The problem of finding a curve c that minimizes Eq. (36) is known as the calculus of variation problem. The curve must satisfy the following Euler-Lagrange equation:

$$\alpha c''(s) + \beta c''''(s) - \lambda \frac{dE_{ex}}{dc} = 0 \,. \tag{40}$$

One much discussed point about snakes is their inability to find the boundary when the initial contour is placed too far away from the actual boundary location. One solution is increasing σ in Eq. (39) to allow the snake to come to equilibrium from a longer range at coarse scale and then slowly reducing σ to allow tracking of the boundary at a finer scale.

Another solution proposed by Xu and Prince (1997) is a gradient vector field (GVF), which is a diffusion of image edge map. Let e be the edge map of image f. The GVF v=(u, v) is the vector field that minimizes the following energy function:

$$E = \int\int \mu({u_x}^2 + {u_x}^2 + {u_x}^2 + {u_x}^2) + |\nabla e|^2 |\,\mathrm{v} - \nabla e|^2 \; dxdy \tag{41}$$

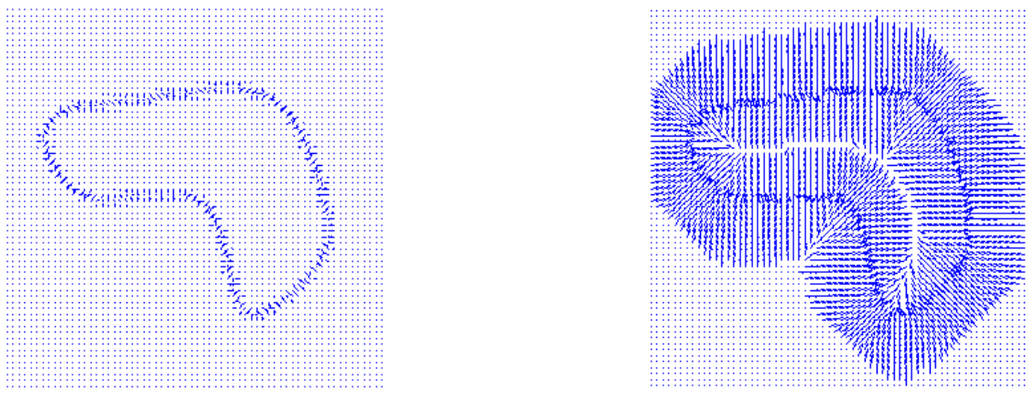

Fig. 8. An edge map (left) and its gradient vector field (right). Gradient vector field basically is the diffusion of the edge map. This allows the contour points to be pulled to the edge from longer distance.

Thus, even in the homogeneous regions of the image, the GVF has vectors that vary smoothly and point toward edges. This diffused field replaces the $-\nabla E_{ex}$ in Eq. (40) to guide the positioning of the snake. Fig. 8 shows an example of an original map and its gradient vector field.

The snake is always attracted to the strong edge in the above external image forces. However, this may not be good behavior for medical image segmentation. For example, the active contour for the lower contrast boundary may be attracted to the nearby higher contrast structures (Fig. **9**). To solve this problem, Fenster and Kender (2001) used a statistical image energy function. The statistical term measures the distance between the distributions of the intensities and gradients along the contour sector's normal direction and the distributions from training data. Let the two image features defined in this method be

$$\begin{aligned} f_c &= f(c(s)) \\ \nabla f_{c^\perp} &= c^\perp(s) \cdot \nabla f(c(s)). \end{aligned} \tag{42}$$

Assume that the distributions of the two image features are normal: $N(\mu_1, \sigma_1)$ and $N(\mu_2, \sigma_2)$. Here μ and σ are given and obtained from the training contours. Then, the external energy of the active contour is defined as

$$E_{ex} = \int \frac{(f_c - \mu_1)^2}{{\sigma_1}_c^2} + \frac{(\nabla f_{c^\perp} - \mu_2)^2}{\sigma_2^2} ds. \tag{43}$$

3.2 Non-parametric deformable model (level set, geometric active contour)

The parametric deformable model has difficulty handling the change in topology of the unknown object to be segmented. Non-parametric deformable models are based on curve convolution theory and level set methods (Osher and Sethian 1988, Sethian 1999.) The curve is represented implicitly as a level set function with the extra dimension of time. The evolution of curve and surface is independent of parameterization and, therefore, the topological changes can be handled automatically.

Given a level set function with the moving curve u as its zero level set at any time t, we have

$$\phi(u(t), t) = 0. \tag{44}$$

Fig. 9. Active contour to segment a phantom's spine is attracted by the stronger edges of the surrounding bones.

Using the chain rule, we have

$$\frac{\partial \phi}{\partial t} + \nabla \phi \cdot \frac{\partial u}{\partial t} = 0. \tag{45}$$

In contour evolution theory, the evolution of the contour along its normal direction can be characterized by the following equation:

$$\frac{\partial u}{\partial t} \cdot n = F \tag{46}$$

where n is an inward unit normal and F is a speed function that determines the speed of the moving curve. Assuming that $\phi < 0$ inside the zero level set curve and $\phi > 0$ outside, the inward unit normal to the level set curve is given by

$$n = -\frac{\nabla \phi}{|\nabla \phi|} \tag{47}$$

With Eq. (45) and Eq. (46), Eq. (47) can be converted into the following final *curve evolution equation*:

$$\frac{\partial \phi}{\partial t} = F|\nabla \phi| \tag{47}$$

The two most common and most-studied deformations in curve evolution theory are curvature deformation and constant deformation. Their respective speed functions are given by:

$$F = \varepsilon k, \text{ where } \varepsilon \text{ is a positive constant and } k \text{ is the curvature , and} \tag{48}$$

$$F = V_0, \text{ where } V_0 \text{ is a constant .} \tag{49}$$

The curvature k at zero level set is given by

$$k = \nabla \cdot \frac{\nabla \phi}{|\nabla \phi|} = \frac{\phi_{xx}\phi_y^2 - 2\phi_x\phi_y\phi_{xy} + \phi_{yy}\phi_x^2}{\left(\phi_x^2 + \phi_y^2\right)^{3/2}}. \tag{50}$$

In the application of image segmentation, most non-parametric deformable model methods allow the curve evolution equation to be modified in two ways: changing the speed function F and adding additional constraints. A good survey of these methods is provided by Suri et al. (2002). Some methods that include regional terms will be reviewed in the next section.

Caselles et al. (1993) and Malladi et al. (1995) independently proposed a geometric active-contour model based on the following curve evolution equation:

$$\frac{\partial \phi}{\partial t} = c(x)(k + V_0)|\nabla \phi| . \tag{51}$$

Here $c(x)$ is

$$c(x) = \frac{1}{1 + |\nabla (G_\sigma (x) * f(x)|} . \tag{52}$$

$c(x)$ can be viewed as a stopping force based on the edge image feature. This multiplicative term slows down the moving curve when the curve is near the boundary. A problem with this model is that if the boundary has gaps or is blurry the curve passes the boundary and will not be pulled back to the correct boundary. Caselles et al. (1997) and Yezzi et al. (1997) add an additional term in the equation that allows the curve to be pulled back:

$$\frac{\partial \phi}{\partial t} = c(x)(k + V_0)|\nabla \phi| + \nabla c \cdot \nabla \phi . \tag{53}$$

Note that $\nabla c = -|\nabla G_\sigma * f|$ behaves like the external force of active contour model in Eq. (39). It attracts the curve to the boundary and is projected onto the normal direction of the contour propagation front so that the curve can be pulled back if it passes the boundary. Fig. **10** illustrates this idea.

3.3 Summary for boundary based methods

The advantage of boundary based methods, in particular, the contour evolution methods, is the piece-wise continuity. Active contour methods are quite sensitive to the initial conditions and cannot handle changes in contour topology. Level set methods, on the other hand, handle the topology problem naturally through the implicit zero level set function. They, however, are more computationally expensive due to the iterative optimization methods for solving complex PDE. With the increasing energy or force terms introduced in these methods, users need to specify the parameters used in these terms that are not easily understandable. This makes the algorithms unintuitive to users in clinical practice.

4. Hybrid methods

Hybrid methods use both boundary and regional information for image segmentation. Many of them are the deformable models discussed in previous sections with extensions that include regional information level set methods with regional forces (4.1). Recently developed methods view image segmentation as a graph partition problem that minimizes an energy function (4.2) and is coupled with a purely statistical framework (4.3).

4.1 Level set methods with regional forces

These algorithms modify the propagation speed V_0 in the original level set segmentation to include a regional force. An elegant example is provided by Baillard et al. (2000). In this approach, probability density functions inside and outside the structure are responsible for creating a pull/push force on the propagating front.

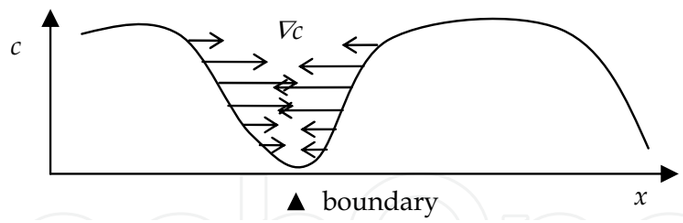

Fig. 10. Pull back force. The arrows show the gradient of c in Eq (53).

Let $g(x) \in \{\text{in, out}\}$ be the two classes of regions, let $p_{in}(y)$ be the probability density function of gray-level y to be estimated inside the curve, and $p_{out}(y)$ be the probability density function outside the curve. The bi-directional propagation force is estimated as

$$V_0 = sign\{\alpha p_{in}(y) - (1-\alpha)p_{out}(y)\}. \tag{54}$$

Here, $sign(z) = 1$ if $z \geq 0$, otherwise $sign(z) = -1$. This determines the moving direction of a voxel on the propagation front based on the probability that it belongs to the outside or the inside region. The stopping force $c(x)$ in Eq. (51) is also modified to be

$$c(x) = t(P_T(x \mid f, g)), \tag{55}$$

where,

$$t(p) = \begin{cases} 1 - 4p^3 & \text{if } p < 0.5 \\ 4(1-p)^3 & \text{otherwise} \end{cases}, \text{ and} \tag{56}$$

$$P_T(x \mid f, g) = \begin{cases} \dfrac{(1-\alpha)p_{in}(f(x))}{\alpha p_{out}(f(x)) + (1-\alpha)p_{in}(f(x))}, \text{if } g(x) = \text{out} \\ \dfrac{\alpha p_{out}(f(x))}{\alpha p_{out}(f(x)) + (1-\alpha)p_{in}(f(x))}, \text{if } g(x) = \text{in} \end{cases}. \tag{57}$$

P_T is called the transitional probability. This stopping term can be understood in the following way: if x on the propagation front is outside the curve and the transitional probability shows that it is likely inside the region, then the curve is crossing the boundary. Therefore, the evolution speed will slow down at x. Note that the parameters of probability density functions are estimated adaptively by stochastic-EM (SEM) without the need for training data. The method has shown impressive results for brain image segmentation.

4.2 Graph cut methods that minimize an energy function with both regional and boundary terms

Motivated by Greig's MAP-MRF formulation (1989) of an energy function with regional information and an MRF-shaped smoothness prior, Boykov and Jolly (2001) replace the smoothness term φ_2 in Eq. (34) with a boundary term:

$$E = -\sum_{i=1}^{N} \log(p(y_i \mid x_i)) + \lambda \sum_{i=1}^{N} \sum_{j \in N_i} B_{ij}\delta(x_i, x_j), \tag{58}$$

where B_{ij} is

$$B_{ij} = \exp\left(-\frac{\left|y_i - y_j\right|^2}{2\sigma^2}\right) \cdot \frac{1}{dist(i,j)}. \tag{59}$$

Fig. 11. Graphical model of Conditional Random Fields. Each tuple (y, x_i, x_j) is a maximum clique.

This boundary term encourages strong edges of the target region, that is, if the contrast of intensity between neighboring voxel i and j is high, they are more likely to be assigned to two different classes.

This energy function can be minimized by graph min-s-t cut as well for target object and background two-class segmentation as described in section 2.7.2.2. The method uses an interactive tool to specify the hard constraints via paintbrushes that identify the voxels inside the target region and those outside. Colorization utilizes a similar idea (Levin and Lischinski 2004). For the target or background "seed" voxels specified by the user, a high cost is assigned to the edges connecting those nodes to the class node s or t so that these nodes cannot be partitioned to the other class.

Freedman and Zhang (2005) adopted a similar approach that includes a regional term derived from the probabilistic atlas as a shape prior. The position of the voxel is included as the image feature and is used to estimate the probability of where the voxel resides as the target or background region from the probabilistic atlas in the training data.

4.3 Condition Random Fields

The major drawback of using MRF as a model for labeling voxels (unknown data) is the difficulty of using intensity information (observed data) around the voxel's neighbors. To make use of the information, independence assumptions about the observation samples must be modeled. The problem is addressed by Lafferty et al. (2001) with the formation of a formal extension of MRF called Conditional Random Field (CRF).

CRF is an MRF, but globally conditioned by the observed image y. This is accomplished by including y in the undirected graphical model and connecting y to all the unknown random variables of x in the random field (Fig. **11**). Thus, each tuple of $\{(y, x_i, x_j) \mid i \neq j, j \in N_i\}$ is a maximum clique. Similar to Eq. (31) and (32) in MRF, using the Hammersley-Clifford theorem, we have

$$p(x \mid y) = \frac{1}{Z} \prod_c \psi_c(x_c, y) , \tag{60}$$

and

$$\psi_c(x_c, y) = \exp(-E(x_c, y)) , \tag{61}$$

The maximum a posterior (MAP) estimation of Eq. (60) is equivalent to minimizing the energy function

Fig. 12. Synthetic image for comparison of Boykov's method and Hu's method. The target is the inner rectangle. The second image shows that Boykov's method is meant to attract high contrast boundaries and thus mis-segment the regions (the two small rectangles.) Additional brush strokes are needed to remove the mis-segmented regions (the third image.) Hu's method correctly segments the target region once the boundary statistics are trained (the fourth image.)

$$E(x,y) = \sum_c E(x_c, y)\,, \tag{62}$$

Similar to Eq. (33), the energy function can then be defined over the clique with respect to voxel i as

$$E(x,y) = \sum_{i=1}^{N} \varphi_1(x_i, y) + \beta \sum_{i=1}^{N} \sum_{j \in N_i} \varphi_2(x_i, x_j, y)\,, \tag{63}$$

With this formation, also motivated by Greig et al. and Boykov et al., Hu et al. (2008) define the following potential functions using the framework of CRF:

$$\begin{aligned} \varphi_1(x_i, y) &= -\ln p(y_i \mid x_i) \\ \varphi_2(x_i, x_j, y) &= -\ln p(y_i, y_j \mid x_i \neq x_j) \end{aligned} \tag{64}$$

Note that φ_1 in the above equation is identical to the regional term in Grieg's and Boykov's energy function, whereas φ_2 can be viewed as a boundary term that describes the probability that neighboring voxels i and j belong to different regions. Those probabilities can be estimated from training data locally during the segmentation process.

With Eq. (64), CRFs become a purely statistical framework for image segmentation. This addresses the problem of Boykov's method using contrast as the boundary term that is sensitive to noise and tends to segment the target object boundary along a high contrast edge (Fig. 12.) This heuristic boundary term is usually not suitable for medical applications.

5. Atlas-based methods

Deformable atlases are adaptable templates that reflect the anatomy of new subjects and thus allow automated segmentation of the structures in new scans. Model-driven methods (e.g., the active shape model) build explicitly geometric models that are parameterized. Segmentation is achieved by adjusting the poses and parameters for controlled deformation in the target image. Intensity driven methods, on the other hand, involve image registration techniques to compute an anatomically correct coordinate transformation between a target image and an already segmented image. We will discuss these two approaches in general in the following two sections.

5.1 Atlas as average shape: active shape model/active appearance model

The active shape model (Cootes and Taylor 1992) constructs a shape prior model to enhance the performance of deformable models. By aligning training shapes in the same model space and using principal component analysis (PCA), any shape Y (set of landmark points) in the training set can be approximated by

$$Y \approx \tilde{Y} + Pb^T, \tag{65}$$

where P is the matrix of the first m eigenvectors and b=(b_1, b_2, ..., b_m) is the weighting vector – the shape parameters. Initially, the mean shape $\tilde{Y}$ is used as the initial curve in the new scan. The deformation is computed using the standard deformable models described in Section 3. At each iteration, the displacement from the curve in the previous iteration is used to calculate the corresponding pose (rotation, translation, and scale), as well as the shape parameters, to obtain a new curve to be deformed in the next iteration. In this way, only deformations that are similar to the shapes in the training set are allowed. The iterations stop when the changes of poses and shape parameters are not significant.

The active appearance model (Cootes at al. 1998) extends this paradigm to incorporate the image intensity prior along with the shape prior, i.e.,

$$g \approx \tilde{g} + P_g b_g{}^T. \tag{66}$$

To obtain these intensity parameters, image registration between the training data is needed. Further, PCA is applied to the combined shape and intensity parameters.
Instead of using a set of landmark points on the surface of the target object as the representation of the shape, Pizer et al. (2003) used a medial axis shape representation. The shape is represented by a set of "atoms" on the medial axis (sheet in 3D), with arms extended to control the surface formation. Instead of calculating the pose and parameters of the shape as in the active shape model, the pose and parameters of the atoms are calculated. The major advantage of this shape representation is scalability of the surface mesh. Thus, multi-scale deformation is possible.

5.2 Atlas as individual image

In this approach, an atlas is a spatial map of anatomical structures, which is usually derived from a reference image by manual segmentation. The automatic segmentation is generated by registering an image to an atlas, that is, by computing a correct coordinate mapping between the two. Then the voxels can be labeled according to the transformation mapping.

An intensity similarity measure is chosen, such as cross correlation or the more robust mutual information (MI) (Maes et al. 1997), for the registration. The displacement field is obtained by minimizing the differences between the two images based on the similarity measure with some smoothness constraints on the displacement field. The smoothness constraints can be determined using a Gaussian or an elastic model, such as thin-plate and viscous-fluid. Image registration itself is a subject of active research. Pluim and Fitzpatrick (2003) give a review of image registration methods.

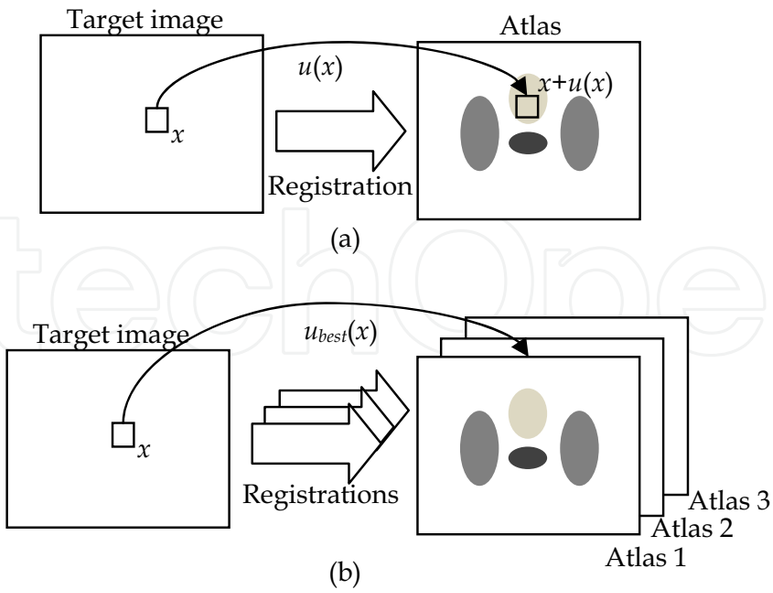

Fig. 13. (a) Atlas-based segmentation using a single atlas. Each voxel is displaced into the atlas based on the displacement field u from the registration and labeled accordingly. (b) Using multiple atlases, one registration is done for each atlas. The best registration is used to label the voxel.

The most straightforward strategy for selection of an atlas is to use a segmented image from a single (model) individual (Fig. **13**(a)). The strategy could be random or based on such heuristic criteria such as image quality or normality of the subject. One can also use multiple individual atlases to register the target image one by one and choose the best atlas for segmentation (Fig. **13** (b)). Usually, the accessible number is the final value of the registration criterion or image similarity measure.

In the pattern recognition community, multiple independent classifiers can be combined and together consistently achieve classification accuracy. Rohlfing and Maurer (2004) use the same concept to combine the results from multiple atlases to obtain the final segmentation. The coordinate transformation of registration is continuous and does not map grid points of the image to grid points in the atlas. Therefore, interpolation is required. The simplest interpolation is nearest-neighbor interpolation. A more sophisticated technique used to label data is partial volume (PV) interpolation, originally proposed by Meas et al. to generate histograms used for MI. The voxel is labeled based on a frequency histogram of labels from multiple atlases displaced within the voxel's volume. Let H_x be the frequency histogram for the labels of voxel x on the target image, for a registration u; the histogram is updated as follows

$$\begin{aligned} &H_x(L_k(x+u(x))) = H_x(L_k(x+u(x))) + w_k, k = 1,2,3,4 \text{ for 2D} \\ &w_k = d_k / \sum_{i=1}^{4} d_i, \end{aligned} \tag{67}$$

where L_k is the label of the four (2D) voxels forming the cell that contains $x+u(x)$, and d_k is the distance from $x+u(x)$ to these voxels. The best label for a voxel is the label that has highest frequency.

6. Discussion

No single method can best handle all the anatomic structures in medical image segmentation. Typically, methods discussed in this survey are modified to segment a particular structure; or a method can take advantage of other methods to serve an intermediate purpose.

Threshold-based methods are the fastest, simplest, and easiest to implement, so they are still indispensable in modern commercial software. They are useful for segmenting structures that have separated intensity distribution from the other structures. Such structures are the outer body, lung, and bone. The drawback of thresholding is that it does not guarantee piecewise continuity and is sensitive to the artifacts mentioned in section 1. However, it can be used as a starting point for other methods, such as seed points for region growing.

Region-growing methods are also fast if the mean intensity is used in the region homogeneity predicate, and therefore an interactive tool can be implemented. Region-growing methods also guarantee piecewise continuity, work quite well in finding high-contrast boundaries, and are less sensitive to noise then thresholding. The major problem is leakage if the boundary is blurred, and they are sensitive to start point position.

Cluster-based methods are easy to implement and perform well with a spatial constraint, especially for MR brain image segmentation. They may not work on CT images, since the intensity distributions of many organs overlap (Table 1.) Just like thresholding, clustering-based methods could also be used as a starting point for other techniques, such as generating an initial contour for a deformable model.

Deformable model-based methods are very popular in medical imaging. These methods also guarantee piecewise continuity, and with level set methods, the topology changes are handled naturally. Deformable model-based methods incorporating statistical regional information show promising results. However, many of them require tuning the parameters; and there is a trade-off between convergence speed and stability under the iterative optimization scheme.

Graph cut-based methods that minimize an energy function are fast and guarantee that one will find a global optimum for two-class segmentation. The results show the advantages (Hu et al. 2008) of using a probabilistic framework, such as conditional random fields (CRFs), with both statistical regional and boundary potentials. Unfortunately, multiple region segmentation using graph cut (K-cut) is NP hard (recently, Grady (2006) used a random walker for multiple region segmentation based on graph cut theory). However, multiple region segmentation can be done recursively by the two-class segmentation. This framework can also incorporate other methods, such as an atlas for additional regional properties.

Model-driven, atlas-based methods are not prone to noise and leakage because of the shape constraints from the training set. The major drawbacks are that the intensive labor for building the training set and matching the model to the image can be time-consuming, especially for complex structures that require many shape and intensity parameters to be calculated. The image registration-based atlas method is straightforward. However, it is based on image similarity and can be adversely affected when structures, such as air cavities, surgical implants, or surgically removed structures, differ between target and study images. The best application of these methods is intra-patient segmentation, such as in 4D CT images. One can segment the anatomic structures in the image set at one respiration phase, then propagate the segmentations by registration to the images at other phases (Pevsner et al. 2006). This procedure is extremely useful for studying organ or tumor motion and deformation during the treatment session.

In conclusion, the fundamental aspects of medical images -- the modalities of image acquisition, complexity of anatomical structures, the non-rigid nature of organ motion and deformation -- and increasing information from advanced modern imaging techniques make the segmentation difficult and challenging. It may not be possible to delineate certain structures without some degree of anatomical knowledge by a human, let alone with a computer. Hybrid methods, with both regional and boundary features, that utilize statistical information and are guided by expert users should shape the future of automatic medical image segmentation.

7. References

Aboutanos, G.B.; Nikanne, J.; Watkins, N. & Dawan, B.M. (1999). Model creation and deformation for the automatic segmentation of the brain in MR images. *IEEE Trans on Biomedical Engineering*, Vol. 46, Issue 11, Nov. 1999, 1346 – 1356, ISSN: 0018-9294.

Adams, R. & Bischof, L. (1994). Seeded region growing. *IEEE Trans. on Pattern Analysis and Machine Intelligence*, Vol. 16, Issue 6, June 1994, 41-647, 1994, ISSN: 0162-8828.

Baillard, C.; Hellier, P & Barillot, C. (2000). Segmentation of 3-D Brain Structures Using Level Sets. *Research Report 1291, IRISA*, Rennes Cedex, France, 16 pages, Jan. 2000.

Besag, J. (1986). On statistical analysis of dirty pictures. *J. of the Royal Statistical Society*. Series B, vol. 48, no.3, 1986, 259-302, ISSN: 1369-7412.

Bezdek, J.C. (1981). *Pattern Recognition with Fuzzy Objective Function Algorithms*. Plenum Press, New York, 1981, ISBN: 0-3064-0671-3.

Boykov, Y. & Jolly, M.P. (2001). Interactive graph cuts for optimal boundary & region segmentation of objects in N-D images. *Proc. of Int. Conf. Computer Vision*, pp. 105-112, 2001.

Caselles, V.; Catte, F.; Coll, T. & Dibos, F. (1993). A geometric model for active contours, *Numerische Mathematik*, Vol. 66, No. 1, 1993, 1-31, ISSN: 0029-599X.

Caselles, V.; Kimmel, R. & Shapiro, G. (1997). Geodesic Active Contours, *Int. J. of Computer Vision*, Vol. 22, No. 1, 1997, 61-79, ISSN: 0920-5691.

Chuang, K.S.; Tzeng, H-L; Chen, S.; Wu, J. & Chen, T-J. (2006). Fuzzy c-means clustering with spatial information for image segmentation, *Computerized Medical Imaging and Graphics*, Vol. 30, No. 1, Jan. 2006, 9-15, ISSN: 0895-6111.

Dempster, A.; Laird N. & Rubin, D. (1977). Maximum likelihood from incomplete data via the EM algorithm. *J. of the Royal Statistical Society*, Series B, Vol. 49, No. 1, 1977, 1-38, ISSN: 1369-7412.

Fenster, S.D. & Kender, J.R. (2001). Sectored snakes: evaluating learned-energy segmentations. *IEEE Trans. on Pattern Analysis and Machine Intelligence*, Vol. 23, Issue 9, Sept. 2001, 1028–1034, ISSN: 0162-8828.

Freedman, D. & Zhang T. (2005). Interactive graph cut based segmentation with shape priors. *Computer Vision and Pattern Recognition, 2005, IEEE Computer Society Conf. on*, Vol. 1, 20-25 June 2005, pp.755 – 762.

Geman, S. & Geman, D. (1984). Stochastic relaxation, Gibbs distributions, and the Bayesian restoration of images. *IEEE Trans. on Pattern Analysis and Machine Intelligence*, Vol. 6, No.6, June 1984, 721-741, ISSN: 0162-8828.

Grady, L. (2006). Random walker for image segmentation. *IEEE Trans. on Pattern Analysis And Machine Intelligence*, Vol. 28, No. 11, Nov. 2006, 1768-1783, ISSN: 0162-8828.

Greig, D.; Porteous, B. & Seheult, A. (1989). Exact maximum a posteriori estimation for binary images. *J. of the Royal Statistical Society*, Series B, Vol. 51, 1989, 271-279, ISSN: 1369-7412.

Horowitz, S.L. & Pavlidis, T. (1974). Picture segmentation by a directed split-and-merge procedure. *Proceedings of the 2nd Int. Joint Conf. on Pattern Recognition.* 1974, pp. 424-433.

Hu, Y.C.; Grossberg, M. D. & Mageras, G. S. (2008). Semi-automatic medical image segmentation with adaptive local statistics in Conditional Random Fields framework. *Proceeding of 30th Annual Int. Conf. of Engineering in Medicine and Biology Society*, Aug. 2008, pp. 3099-3102.

Kapur, J.N.; Sahoo, P.K. & Wong A.K.C. (1985). A new method for gray-level picture thresholding using the entropy of the histogram. *Computer Vision, Graphics, and Image Processing* , Vol. 29, 1985, 273–285, ISSN: 0734-189X.

Kass, M.; Witkin, A. & Terzopoulos, D. (1988). Snakes: active contour models. *Int. J. of Computer Vision*, Vol. 1, 1988, 321-331, ISSN: 0920-5691.

Kolmogorov, V. & Zabih, R. (2004). What energy functions can be minimized via graph cuts? *IEEE Trans. on Pattern Analysis and Machine Intelligence*, Vol. 26, Issue 2, Feb. 2004, 147-159, ISSN: 0162-8828.

Lafferty, J.; McCallum, A. & Pereira, F. (2001). Conditional random fields: Probabilistic models for segmenting and labeling sequence data. *Proceeding of 18th Int. Conf. on Machine Learning,* 2001, pp.282–289.

Levin, A.; Lischinski, D. & Weiss, Y. (2004). Colorization using optimization. *ACM SIGGRAPH 2004*, 2004, pp.689-694.

Lin, Z.; Jin, J. & Talbot, H. (2001). Unseeded region growing for 3D image segmentation. *ACM Int. Conf. Proceeding Series; Vol. 9, Selected papers from Pan-Sydney Workshop on Visual Information Processing*, Sydney, Australia, 2001, pp. 31-37.

Lloyd, S. (1982). Least squares quantization in PCM. Special issue on quantization, *IEEE Trans. Information Theory*, Vol. 28, Issue 2, Mar. 1982, 129–137, ISSN: 0018-9448.

Maes, F.; Collignon, A.; Vandermeulen, D.; Marchal, G & Suetens, P. (1997). Multimodality image registration by maximization of mutual information, *IEEE Trans on Medical Imaging*, Vol. 16, Issue 2, April 1997, 187-198, ISSN: 0278-0062

Malladi, R.; Sethian, J. & Vemuri, B.C. (1995). Shape modeling with front propagation: A level set approach. *IEEE Trans on Pattern Analysis and Machine Intelligence*, Vol. 17, Issue. 2, Jan. 1995, 158-175, ISSN: 0162-8828.

Mohamed, N.A.; Ahmed, M.N. & Farag, A. (1999). Modified fuzzy c-mean in medical image segmentation. *In Proceeding IEEE Int. Conf. on Acoustics, Speech, and Signal Processing 1999*, Vol. 6, Mar. 1999, pp.3429-3432.

Osher, S. & Sethian, J.A. (1988). Fronts propagating with curvature-dependent speed: Algorithms based on Hamilton-Jacobi formulations. *J. of Computational Physics*, Vol. 79, 1988, 12-49, ISSN: 0021-9991.

Otsu, N. (1979). A threshold selection method from grey-level histograms. *IEEE Trans. on Systems, Man, and Cybernetics*, Vol. 9, Issue 1, Jan 1979 , 62–66, ISSN: 0018-9472.

Pevsner, A.; Davis, B.; Joshi, S.; Hertanto, A., Mechalakos, J.; Yorke, E.; Rosenzweig, K.; Nehmeh, S.; Erdi, Y.E.; Humm, J.L.; Larson, S.; Ling, C.C. & Mageras, G.S. (2006). Evaluation of an automated deformable image matching method for quantifying lung motion in respiration-correlated CT images. *Medical Physics*, Vol. 33, No. 2, Feb. 2006, 369-376, ISSN: 0094-2405.

Pham, D.L. (2002). Fuzzy clustering with spatial constraints. *In Proceedings of the IEEE Int. Conf. on Image Processing*, New York, USA, August, 2002, pp.65-68.

Pizer, S.M.; Fletcher, P.T.; Joshi, S.C.; Thall, A.; Chen, J.Z.; Fridman, Y.; Fritsch, D.S.; Gash, A.G.; Glotzer, J.M.; Jiroutek, M.R.; Lu, C.; Muller, K.E.; Tracton, G.; Yushkevich, P.A. & Chaney, E.L. (2003). Deformable M-Reps for 3D Medical Image Segmentation. *Int. J. of Computer Vision,* Vol. 55, Issue 2-3, Nov.-Dec. 2003, 85-106, ISSN: 0278-0062.

Pluim, J.P.W. & Fitzpatrick, J.M. (2003). Image registration. *IEEE Trans on Medical Imaging*, Vol. 22, Issue 11, Nov. 2003, 1341-1343, ISSN: 0278-0062.

Ridler, T. & Calvard, S. (1978). Picture thresholding using an iterative selection method. *IEEE Trans. on Systems, Man, and Cybernetics*. Vol. 8, 629–632, ISSN: 0018-9472.

Rohlfing, T. & Maurer, C.R. Jr. (2004). Multi-classifier framework for atlas-based image segmentation. *Computer Vision and Pattern Recognition, 2004, IEEE Computer Society Conf. on,* Vol. 1, 27 June-2 July 2004, 255-260.

Rosenfeld, A. & Torre, P.D.L. (1983). Histogram concavity analysis as an aid in threshold selection, *IEEE Trans. on Systems, Man, and Cybernetics*, Vol. 13, 1983, 231–235, ISSN: 0018-9472.

Sethian, J.A. (1999). *Level Set Methods and Fast Marching Methods*. Cambridge University Press, 2nd edition, 1999, ISBN: 0-5216-4557-3.

Sezan, M.I. (1990). A Peak detection algorithm and its application to histogram-based image data reduction. *Computer Vision, Graphics, and Image Processing*, Vol. 49, 1990, 36-51, ISSN: 0734-189X.

Sezgin, M. & Sankur, B. (2004) Survey over image thresholding techniques and quantitative performance evaluation. *J.of Electronic Imaging*, Vol. 13, No. 1, 2004, 146-168, ISSN: 1017-9909.

Sonka, M. & Fitzpatrick, J.M. Eds. (2000). *Handbook of Medical Imaging. Vol. 2. Medical image Processing and Analysis*. SPIE press, 2000, ISBN: 0-8194-3622-4

Suri, J.S.; Liu, K.; Singh, S.; Laxminarayan, S.N.; Zeng, X. & Reden, L. (2002). Shape recovery algorithms using level sets in 2-D/3-D medical imagery: A state-of-the-art review. IEEE *Trans. on Information Technology in Biomedicine*, Vol. 6, Issue 1, March 2002, 8 – 28, ISSN: 1089-7771.

Xu, C. & Prince, J.L. (1997). Gradient vector flow: A new external force for snakes. *Computer Vision and Pattern Recognition 1997, IEEE Computer Society Conf. on,* 1997, pp. 66-71.

Yezzi, A.; Kichenassamy, S.; Kumar, A.; Olver, P. & Tannenbaum, A. (1997). A geometric snake model for segmentation of medical imagery, *IEEE Trans on Medical Imaging*, Vol. 16, Issue 2, April 1997, 199-209, ISSN: 0278-0062.

Biomedical Engineering

Edited by Carlos Alexandre Barros de Mello

ISBN 978-953-307-013-1

Hard cover, 658 pages

Publisher InTech

Published online 01, October, 2009

Published in print edition October, 2009

Biomedical Engineering can be seen as a mix of Medicine, Engineering and Science. In fact, this is a natural connection, as the most complicated engineering masterpiece is the human body. And it is exactly to help our “body machine” that Biomedical Engineering has its niche. This book brings the state-of-the-art of some of the most important current research related to Biomedical Engineering. I am very honored to be editing such a valuable book, which has contributions of a selected group of researchers describing the best of their work. Through its 36 chapters, the reader will have access to works related to ECG, image processing, sensors, artificial intelligence, and several other exciting fields.

INTECH

open science | open minds

InTech Europe

University Campus STeP Ri
Slavka Krautzeka 83/A
51000 Rijeka, Croatia
Phone: +385 (51) 770 447
Fax: +385 (51) 686 166
www.intechopen.com

InTech China

Unit 405, Office Block, Hotel Equatorial Shanghai
No.65, Yan An Road (West), Shanghai, 200040, China
中国上海市延安西路65号上海国际贵都大饭店办公楼405单元
Phone: +86-21-62489820
Fax: +86-21-62489821

IntechOpen